Electronic Transport in Graphene Heterostructures

Andrea F. Young and Philip Kim

Department of Physics, Columbia University, New York, New York 10027;
email: andrea@phys.columbia.edu, pk2015@columbia.edu

Annu. Rev. Condens. Matter Phys. 2011. 2:101–20

First published online as a Review in Advance on December 9, 2010

The *Annual Review of Condensed Matter Physics* is online at conmatphys.annualreviews.org

This article's doi:
10.1146/annurev-conmatphys-062910-140458

1947-5454/11/0310-0101$20.00

Keywords

electronic transport, graphene, quantum Hall effect, p-n junction, Klein tunneling

Abstract

The elementary excitations of monolayer graphene, which behave as massless Dirac particles, make it a fascinating venue in which to study relativistic quantum phenomena. One notable example is Klein tunneling, a phenomena in which electrons convert to holes to tunnel through a potential barrier. However, the omnipresence of charged impurities in substrate-supported samples keep the overall charge distribution nonuniform, obscuring much of this "Dirac" point physics in large samples. Using local gates, one can create tunable heterojunctions in graphene, isolating the contribution of small regions of the samples to transport. In this review, we give an overview of quantum transport theory and experiment on locally gated graphene heterostructures, with an emphasis on bipolar junctions.

1. OVERVIEW

Over the past 20 years there has been a tremendous interest in the electronic properties of low-dimensional condensed matter systems. The interest in these systems stems from the fact that they can manifest novel quantum effects as device dimensions approach fundamental microscopic length scales such as the electronic mean free path or phase coherence length. The quantum properties of such systems are usually described by the nonrelativistic Schrödinger equation, in which quasiparticles have a finite effective mass. Recently, some of that focus has turned to another class of condensed matter systems: graphene, a single atomic layer of graphite. In graphene, the transport properties are described by a relativistic Dirac equation in which the quasiparticles have exactly zero effective mass (1). This relation to relativistic quantum mechanics has provided an interesting theoretical playground for implementing tests of quantum electrodynamics in a simple experimental situation (2).

In this review, we focus on the electronic transport in graphene devices in which the local carrier concentration is controlled by one or more local gates. The nature of transport through these devices depends on the relationship between the length scale on which density changes and the length scale characterizing disorder scattering. In the cleanest devices, transport signatures of the relativistic nature of the graphene quasiparticles are observed. The electronic charge allows the particles to be manipulated by a magnetic field; we also discuss magnetotransport in graphene heterojunctions in both the high and low field limits. Although experimentally unrealized, we summarize theoretical results on multigated graphene superlattices, which can form a basis for a new kind of electronic optics based on graphene as an electronic metamaterial.

Carbon atoms in graphene are arranged in a honeycomb lattice. This hexagonal arrangement of carbon atoms can be decomposed into two interpenetrating triangular sublattices related to each other by inversion symmetry. This unique configuration of the carbon atom network leads to an unusual energy dispersion relation near the Brillouin zone corners. The simplest tight-binding model calculation (3) captures the essence of the band structure of graphene $E(\mathbf{k})$, where $\mathbf{k}$ is located in the hexagonal first Brillouin zone reflecting the underlying real lattice symmetry. The valence ($E < 0$) and conduction ($E > 0$) bands touch at the six Brillouin zone corners, of which two sets of points are inequivalent. These two points in the reciprocal lattice ($\mathbf{K}$ and $\mathbf{K}'$), often termed Dirac points, represent a different linear superposition of Bloch wave functions on the two real space sublattices. Taking two atomic orbitals on each sublattice site as basis, the tight-binding Hamiltonian can be simplified near $\mathbf{K}$ (or $\mathbf{K}'$) as

$$\hat{H} = \pm i\hbar v_F \vec{\sigma} \cdot \vec{\nabla}, \qquad 1.$$

where $\vec{\sigma} = (\sigma_x, \sigma_y)$ are the Pauli matrices, $v_F \approx 10^6$ m/s is the Fermi velocity in graphene, and the $+(-)$ sign corresponds to taking the approximation near the $\mathbf{K}(\mathbf{K}')$ point.

The structure of this Dirac equation is interesting for several reasons. First, the resulting energy dispersion near the zone corners is linear in momentum, $E(\mathbf{k}) = \pm\hbar v_F|\mathbf{k}|$, where $\mathbf{k}$ is defined relative to $\mathbf{K}$(or $\mathbf{K}'$). Consequently, the electrons near these two Dirac points always move at a constant speed, given by the Fermi velocity $v_F \approx c/300$ (rather than the real speed of light c). The electron dynamics in graphene are thus effectively relativistic, with the the speed of light substituted by v_F. In a perfect graphene crystal, the Dirac points ($\mathbf{K}$ and $\mathbf{K}'$) are coincident with the overall charge neutrality point because there are two carbon atoms in the unit cell of graphene and each carbon atom contributes one electron to the two bands, resulting in the Fermi energy E_F of neutral graphene lying precisely at the half-filled band. Consequently, either positively or negatively charged carriers are easily induced by the electric field effect, allowing ambipolar electronic transport (4).

The linear energy dispersion relation also leads to a linearly vanishing two-dimensional (2D) density of states near the charge neutrality point at $E = 0$, $\rho_{2D} \propto |\varepsilon_F|$. This differs from that for conventional parabolic 2D systems in which the density of states, at least in the single particle picture, is constant, leading to a decrease in the ability of charge-neutral graphene to screen electric fields (5). Finally, the sublattice symmetry endows the quasiparticles with a conserved quantum number, chirality, corresponding to the the projection of the pseudospin on the direction of motion (2). In the absence of scattering, which mixes the electrons in the graphene valleys, pseudospin conservation forbids backscattering in graphene (6)—momentum reversal is equivalent to the violation of pseudospin conservation. This absence of backscattering has been advanced as an explanation for the higher electron mobility of metallic as compared with semiconducting nanotubes (7), and it is partially responsible for a similar relative difference between mono- and bilayer graphene.

A sudden burst of experimental and theoretical work on graphene followed the first demonstration of single- and multilayered graphene samples made by mechanical extraction (8–11) and chemical synthesis (12). Since this discovery, numerous unique electrical, chemical, and mechanical properties of graphene have been investigated. In particular, an unusual half-integer quantum Hall (QH) effect and a nonzero Berry's phase (4, 13) were discovered in graphene, providing unambiguous evidence for the existence of Dirac fermions in graphene and distinguishing graphene from conventional 2D electronic systems with a finite carrier mass. Comprehensive graphene reviews, of varying degrees of generality, exist (14–22). In this review, we focus on the electronic transport properties of graphene in the presence of gate-induced static electrical potentials. As we discuss below, by varying the potential on scales smaller than the electronic mean free path, experiments can probe graphene-specific effects that are obscured in bulk transport, which is often dominated by inhomogeneity. In particular, sharp potential modulations can produce sharp bipolar junctions. These p-n junctions merit study both because they constitute a key ingredient for potential device applications built on electronic lensing (23) and because they represent a critical component of the transport landscape of charge neutral graphene (24, 25).

The observation of electron and hole puddles in charge-neutral, substrate-supported graphene (25) confirmed theoretical expectations (24) that transport at charge neutrality is dominated by charged impurity-induced inhomogeneity (26–28). The picture of transport at the Dirac point results from conducting puddles separated by a network of p-n junctions. Understanding the properties of graphene p-n junctions is thus crucial to quantitative understanding of the minimal conductivity, a problem that has intrigued experimentalists and theorists alike (4, 24, 28–33). Describing transport in the inhomogeneous potential landscape of the charge neutrality point requires introduction of a spatially varying electrical potential into Equation 1; transport across a p-n junction corresponds to this potential crossing zero. Because graphene carriers have no mass, graphene p-n junctions provide a condensed matter analog of the so-called Klein tunneling problem in quantum electrodynamics. The first part of this review is devoted to a theoretical understanding of ballistic and diffusive transport across such as barrier.

In recent years, substantial effort was devoted to improving graphene sample quality by eliminating unintentional inhomogeneity. Some progress in this direction has been made both by suspending graphene samples (34, 35) and by transferring them to single-crystal hexagonal boron nitride (hBN) substrates (36). These techniques have succeeded in lowering the residual density present at charge neutrality, but even the cleanest samples are not ballistic on length scales comparable to the sample size (typically $\gtrsim 1$ μm). An alterative approach is to use local gates to restrict the region of interest being studied.

Graphene's gapless spectrum allows the fabrication of adjacent regions of positive and negative doping through the use of local electrostatic gates. Such heterojunctions offer a simple arena in which to study the peculiar properties of graphene's massless Dirac charge carriers, including chirality (2, 37) and emergent lorentz invariance (38–40). Technologically, graphene p-n junctions are relevant for various electronic devices, including applications in conventional analog and digital circuits (41, 42), as well as novel ones based on electronic lensing (23, 43–45). In the latter part of this review, we discuss current experimental progress toward such gate-engineered coherent quantum graphene devices.

2. REVIEW OF KLEIN TUNNELING IN RELATIVISTIC QUANTUM MECHANICS

One-dimensional (1D) scattering is one of the canonical problems of introductory quantum mechanics. For massive, nonrelativistic particles, the scattering from a finite potential step helps to elucidate fundamental concepts of quantum mechanics such as uncertainty and tunneling. Within little more than a year of Dirac's discovery of the equation for relativistic electrons (46), now known as the Dirac equation, Oskar Klein calculated the barrier transmission problem for relativistic electrons (47). Klein's result was considered paradoxical at the time. In nonrelativistic quantum mechanics, the transmission probability of a particle with energy ε incident on a potential barrier of height $V > \varepsilon$ along the x direction is exponentially decaying with distance, $|T|^2 \sim \exp(-\kappa x)$, where $\kappa > 0$ is a kinetic factor depending on the incident particle's energy and barrier height. In contrast, for the relativistic case, Klein found that the transmission probability does not decay with distance even for $V \gg \varepsilon$, $|T|^2 \sim (4\alpha/(1+\alpha)^2)^2$ (as with κ, here $\alpha \geq 1$ is a kinematic factor obtained from the Dirac equation).

The so-called Klein paradox has two parts. First, far past the barrier, the scattering states are antiparticles or, in the context of condensed matter, holes—a theoretical consequence of the Dirac equation not experimentally confirmed at the time of Klein's calculation (48). Incident particles do not tunnel in the sense of propagating a short distance as evanescent waves; rather, they propagate as antiparticles whose inverted energy-momentum dispersion relation allows them to move freely under the barrier. The second and more subtle part of the paradox is that, even given the existence of holes, tunneling into the barrier should be accompanied by exponential decay of the transmission probability due to the strong repulsive potential at the step. This problem was clarified in 1931 by Sauter, who calculated the transmission of particles over a step with a finite width, finding the expected exponential decay:

$$U(x) = \begin{cases} 0 & x < 0 \\ Fx & 0 \leq x \leq L \\ V & x > L \end{cases} \qquad |T|^2 \sim e^{-2\pi^2 \frac{\hbar c}{F \lambda_C^2}}, \qquad 2.$$

where $\lambda_C = h/(mc)$ is the Compton wavelength and the electric field $F = V/L$. The Klein result of $|T|^2 \sim 1$ obtains for barriers that are sharp compared with the Compton wavelength. The origin of the exponential damping is the existence of regions in the center of the barrier where $\varepsilon - m < V < \varepsilon + m$ and which, as a result, cannot support either electron or hole-propagating states (**Figure 1**). To leading exponential order, the transmission is then given by $T \sim \exp i\int p(x)dx$, where the momentum of the particle in the barrier $p(x) = \pm\sqrt{(U(x)-\varepsilon)^2 - m^2}$ and the integral runs across this classically forbidden region.

Whereas the problem of particles tunneling through and being generated by sharp potential barriers would continue to be applied to physical systems as varied as supercritical atoms and

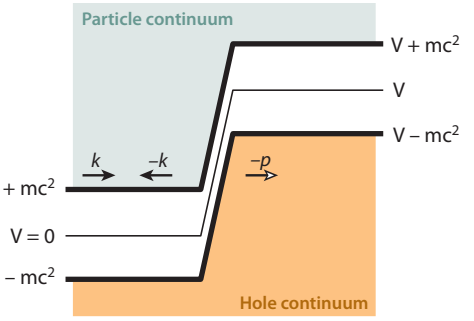

Figure 1

An electron of energy ε scattering off a Klein-Sauter step of height $V > 2m$. The electrons are shown with solid arrowheads; the hole state has a hollow arrowhead. The particle continuum (*top*) and the hole continuum (*bottom*) overlap when $m < \varepsilon < V - m$.

black holes (49), the Klein problem, in its simplest formulation, remained a thought experiment and textbook problem for more than 70 years. The main obstacle in the experimental realization is the creation of potentials varying on the scale of the Compton wavelength, a tall order for bare electrons whose Compton wavelength is $\sim 10^{-12}$ m. In the context of particle physics, such a barrier—effectively achieved in high-energy collisions—quickly leads to physics dominated by the creation of new particles. As discussed in the next section, however, graphene offers a condensed matter realization of the original gedanken experiment in both the Klein and Sauter limits through the study of relativistic single-particle tunneling through controllable potential barriers (for a comprehensive and pedagogical review of the early history of the Klein tunneling problem—from which much of the material in this section is distilled—see Reference 49).

3. KLEIN TUNNELING IN GRAPHENE P-N JUNCTIONS

The approach outlined in Section 2 requires only small modifications to apply to the case of carrier transport across graphene heterojunctions. Although Katsnelson et al. (2) produced the direct calculation for the case of graphene, a similar approach taking into account the chiral nature of carriers had been discussed a decade prior in the context of electrical conduction in metallic carbon nanotubes (6). In low-dimensional graphitic systems, the free particle states described by Equation 1 are chiral, meaning that their pseudospin is parallel (antiparallel) to their momentum for electrons (holes). This causes a suppression of backscattering in the absence of pseudospin-flip nonconserving processes, leading to the higher conductances of metallic over semiconducting carbon nanotubes (7). To understand the interplay between this effect and Klein tunneling in graphene, we introduce external potentials $\vec{A}(\vec{r})$ and $U(\vec{r})$ in the Dirac Hamiltonian,

$$\hat{H} = v_F \vec{\sigma} \cdot \left(i\hbar \vec{\nabla} - e\vec{A}(\vec{r}) \right) + U(\vec{r}). \qquad 3.$$

In the case of a 1D barrier, $U(\vec{r}) = U(x)$, at zero magnetic field, the momentum component parallel to the barrier, p_y, is conserved. As a result, electrons normally incident to a graphene p-n junction are forbidden from scattering obliquely by the symmetry of the potential, while chirality forbids them from scattering directly backward: The result is perfect transmission as holes (2), i.e., Klein tunneling in graphene (see **Figure 2***a*). The rest of this review is concerned with gate-induced p-n junctions in graphene. However, the necessarily transmissive nature of

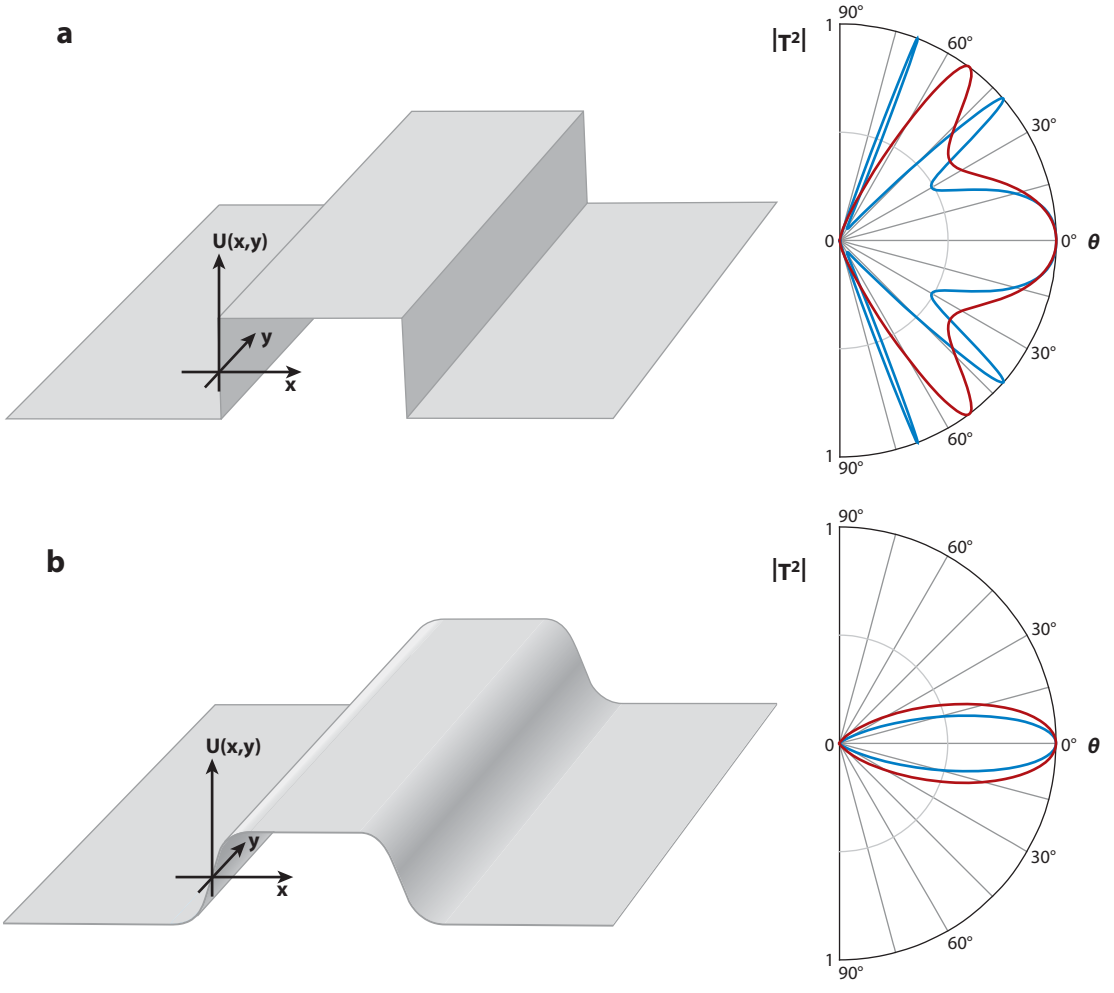

Figure 2

Potential landscape and angular dependence of quasiparticle transmission through (*a*) an atomically sharp pnp barrier and (*b*) an electrostatically generated smooth pnp barrier in graphene, with their respective angle-dependent transmission probability. Red and blue lines correspond to different densities in the locally gated region.

graphene p-n junctions is crucial to understanding the minimal conductivity (33) and supercritical Coulomb impurity (50) problems in graphene. It also plays a role in efforts to confine graphene quantum particles (51). Moreover, p-n junctions appear in the normal process of contacting (52–56) and locally gating (41, 57) graphene, both of which are indispensable for electronics applications.

Even in graphene, an atomically sharp potential cannot be created in a realistic sample. Usually, the distance to the local gate, which is isolated from the graphene by a thin dielectric layer determines the length scale on which the potential varies. Cheianov & Fal'ko (37) solved the resulting transmission problem over a Sauter-like potential step in graphene. Substituting the Fermi energy for the potential energy difference $\varepsilon - U(x) = \hbar v_f k_f(x)$ and taking into account the conservation of the momentum component $p_y = \hbar k_F \sin\theta$ parallel to the barrier, they obtained a result, valid for $\theta \ll \pi/2$, that is nearly identical to that obtained by Sauter (**Figure 2*b***):

$$k_F(x) = \begin{cases} -k_F/2 & x < 0 \\ Fx & 0 \le x \le L \\ k_F/2 & x > L \end{cases} \qquad |T|^2 \sim e^{-2\pi^2 \frac{\hbar v_F}{F_F^2} \sin^2\theta}. \qquad 4.$$

As in the massive relativistic problem in 1D, the transmission is determined by evanescent transport in classically forbidden regions where $k_x(x)^2 = k_F(x)^2 - p_y^2 < 0$ (**Figure 2**). The only differences between the graphene case and the 1D, massive relativistic case are the replacement of the speed of light by the graphene Fermi velocity, the replacement of the Compton wavelength by the Fermi wavelength, and the scaling of the mass appearing in the transmission by the sine of the incident angle. By considering different angles of transmission in the barrier problem in 2D graphene, then, one can access both the Klein and Sauter regimes of $T \sim 1$ and $T \ll 1$.

The current state of the experimental art in graphene does not allow for injection of electrons with definite p_y (58–64). Instead, electrons impinging on a p-n junction have a random distribution of incident angles due to scattering in the diffusive graphene leads. Equation 4 implies that in realistically sharp p-n junctions these randomly incident electrons emerge from the p-n junction as a collimated beam, with most obliquely incident carriers scattering; transmission through multiple p-n junctions leads to further collimation (65). Importantly, even in clean graphene, taking into account the finite slope of the barrier yields qualitatively different results for the transmission: Just as in the original Klein problem, the sharp potential step (2, 66–71) introduces pathologies—in the case of graphene, high transmission at $\theta \neq 0$—which disappear in the more realistic treatment (37, 65, 72).

In fact, the expressions in Equations 2 and 4 are exact for small angles—although the semiclassical approximation used to obtain them is valid only to leading exponential order, the prefactor of T is constrained to a pure phase by the absence of backscattering (6, 7) mentioned above. This allows a quantitative calculation of the ballistic conductance of a graphene p-n junction via the Landauer formula (37)

$$G = \frac{4e^2}{h} \int \frac{W k_F d\theta}{2\pi} |T(\theta)|^2 \approx \frac{2e^2}{\pi h} W \sqrt{\frac{F}{\hbar v_F}}. \qquad 5.$$

For non-phase coherent transport, Equation 5 represents the principal consequence of graphene Klein tunneling p-n junctions.

4. TRANSPORT IN NON-PHASE COHERENT GRAPHENE HETEROSTRUCTURES

Producing clean locally gated samples is the principal experimental challenge that must be overcome to observe Klein tunelling physics in graphene. In particular, if the electrons scatter within the p-n junction, Equation 5 does not hold, as it relies on translational symmetry in the y direction and ballistic electron motion. The condition for the validity of Equation 5 is then that the mean free path ℓ_{MF} should be larger than the p-n junction width L. Crucially, researchers noticed from the first experiments that disordered graphene p-n junctions in general are less resistive than ballistic ones (58, 73), providing a metric for experimental progress. To fulfill $\ell_{MF} > L$, experimental designs have tried to maximize device mobility while minimizing dielectric thickness, which controls the electric field of the p-n junction. Efforts to achieve high-mobility locally gated structures have been manifold, encompassing a zoo of gate dielectrics including cross-linked polymethylmethacrylate (58, 63, 74), high-κ oxides produced by buffered (59, 64, 75) and direct (76) atomic layer deposition, evaporated SiO_2 (77, 78),

vacuum (61, 62), and single-crystal hBN (79). These various techniques lead to mobilities between 100 and 10,000 $cm^2/V{\cdot}sec$ and effective dielectric thicknesses between 5 and 300 nm.

The typical experimental geometry for studying transport in graphene p-n junctions (shown in **Figure 3*a*,*b***) presents a challenge for quantitative study owing to the series resistance of the graphene leads, which contribute to the total resistance even in four terminal measurement schemes. As the voltages on the local top gate and global back gate are tuned, the densities in the locally gated region under the top gate and the graphene leads—the region between the top gate and metal contacts—can be independently tuned, approximately over a range $|n| < 10^{13}$ cm^{-2}. Experimental results for non-phase coherent pnp structures junctions can be summarized by the statement that resistance of the device is higher in the presence of p-n junctions, i.e., $R_{p(-|n|)p} > R_{p(|n|)p}$. Because even in diffusive devices the resistance of graphene

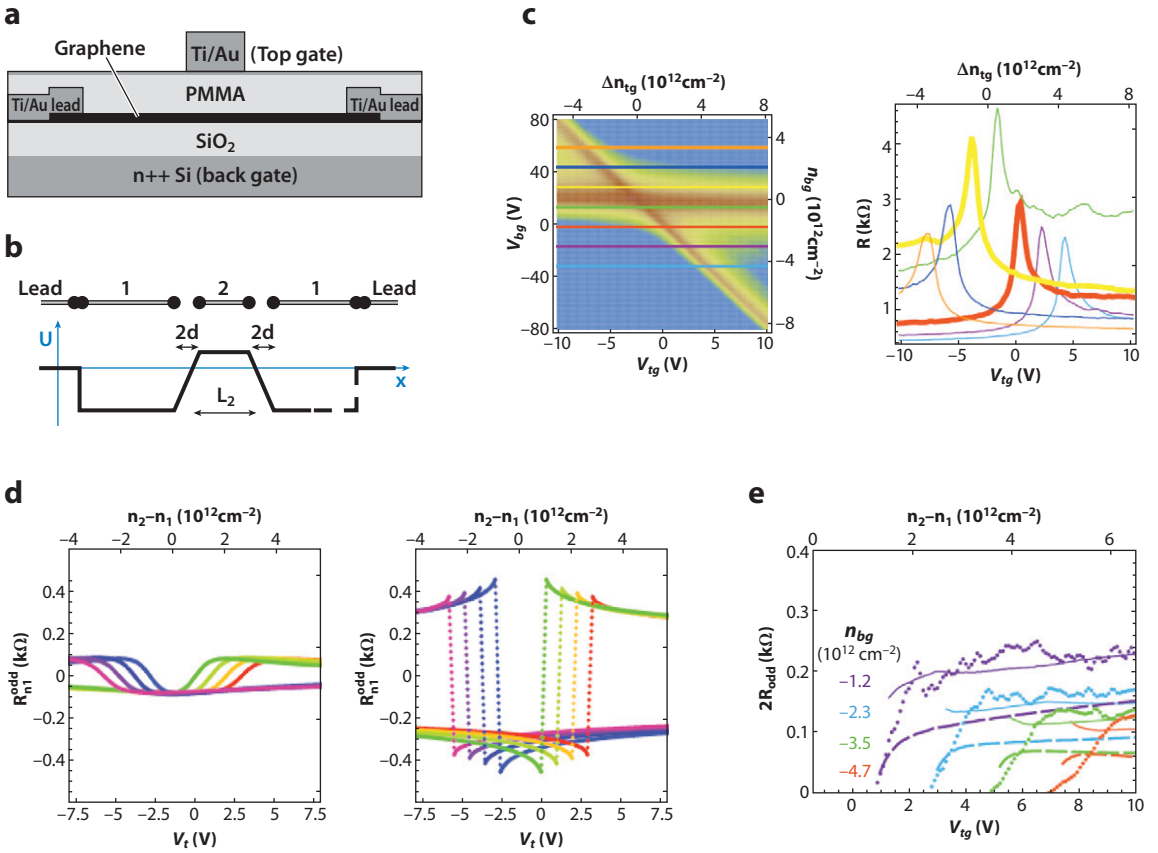

Figure 3

(*a*) Cross-sectional view of a locally gated device and (*b*) a simplified model for the electrochemical potential U of electrons in graphene. The potential is shifted in region 2 by the top-gate voltage and shifted in both regions 1 and 2 by the back-gate voltage. (*c*) Resistance map of the device and fixed back-gate-resistance traces. Resistance is higher in the presence of p-n junctions, upper left and lower right quadrants. Colored lines in the left panel correspond to traces shown in the right panel. (*d*) Calculated R_{odd} for the diffusive (*left panel*) and ballistic (*right panel*) models of a pnp heterojunction for a variety of density imbalances between the p and n regions. Ballistic p-n junctions are more resistive. (*e*) In cleaner devices, a ballistic theory that incorporates nonlinear screening (*solid lines*) (5) provides a good fit to the experimental data (*points*), whereas diffusive theory (*dashed lines*) does not. Reproduced with permission from References 58 and 63.

increases with decreasing doping, the higher resistance of a p-n junction containing channel is not in itself necessarily a consequence of Equation 5. Rather, quantitative analysis of the p-n junction resistance is required.

Due to the electron-hole symmetry of the band structure, the resistance of graphene in most experiments is roughly symmetric with respect to charge conjugation, $R(|n|) \approx R(-|n|)$. This fact can be used to extract the resistance of the p-n junction by constructing the "odd" resistance, $R_{Odd} = R_{p(-|n|)p} - R_{p(|n|)p}$ (58), which measures the isolated resistance of the p-n junctions for potential profiles not too different from those of a parallel plate capacitor. For p-n junctions much shallower than the mean free path ($\ell_{mf} \lesssim L$), charge carriers equilibrate constantly along the channel via scattering. The resulting resistance can be explained by a phenomenological model that takes into account the position dependence of the density and, by extension, the resistivity, $R = \int \rho(x)dx$, $\rho(x) = \left(\sigma_0^2 + (n(x)e\mu)^2\right)$, where σ_0 is the fitting parameter corresponding to the minimal conductivity (58). Early experiments were all firmly in the diffusion-dominated limit (58–60, 80).

Subsequently, simultaneous attempts were made to study Klein phenomena by narrowing the p-n junctions and pnp structures (63, 64) as well as by increasing the device mobility by using air-bridge top gates (61, 62). In both approaches, the details of the potential profile—which, given the inherent requirement that the dielectric thickness be comparable to the length of the top-gated region, deviate strongly from the parallel plate capacitor model—are crucial in analyzing the data in terms of Klein tunneling. This is due to the fundamental problem that in the presence of any scattering, the ballistic and diffusive contributions to the conductance cannot be reliably separated. Nevertheless, in the best samples, a good agreement with Equation 5 was found (see **Figure 3**) (62, 63). Notably, quantitatively accurate fits were not possible without careful consideration of nonlinear screening within the p-n junction (5).

5. PHASE-COHERENT TRANSPORT IN BALLISTIC FABRY-PEROT CAVITIES

Transport measurements across single p-n junctions, or a pnp junction in which transport is not coherent, can, at best, provide only indirect evidence for Klein tunneling by comparison of measured resistance of the p-n junction or junctions against Equation 5. Moreover, because such experiments probe only incident-angle-averaged transmission, they cannot experimentally probe the structure of $T(\theta)$. Thus, although References 53 and 62 show that the resistance of nearly ballistic p-n junctions are in agreement with the ballistic theory, to show that angular collimation occurs, or that perfect transmission occurs at normal incidence, requires a different experiment. In particular, there is no way to distinguish perfect transmission at $\theta = 0$ from large transmission at all angles, begging the question of whether Klein tunneling has any observable consequences outside the context of an angle-resolved measurement or its contribution to bulk properties such as the minimal conductivity. In fact, as Shytov et al. (81) noted, an experimental signature of this phenomenon should manifest as a sudden phase shift at finite magnetic field in the transmission resonances in a ballistic, phase-coherent, graphene pnp device.

Although graphene p-n junctions are transmissive when compared with p-n junctions in gapfull materials (or gapless materials in which backscattering is allowed, such as bilayer graphene), graphene p-n junctions are sufficiently reflective, particularly for obliquely incident carriers, to cause transmission resonances due to Fabry-Perot (FP) interference. However, in contrast to the canonical example from optics, or to 1D electronic analogs (82), the relative phase of interfering paths in a ballistic, phase-coherent pnp (or npn) graphene heterojunction

can be tuned by applying a magnetic field. For the case where the junction width is only somewhat shorter than the mean free path in the locally gated region, $L \lesssim \ell_{LGR}$, the Landauer formula for the oscillating part of the conductance can be derived from the ray-tracing diagrams in Figure 4*d*,

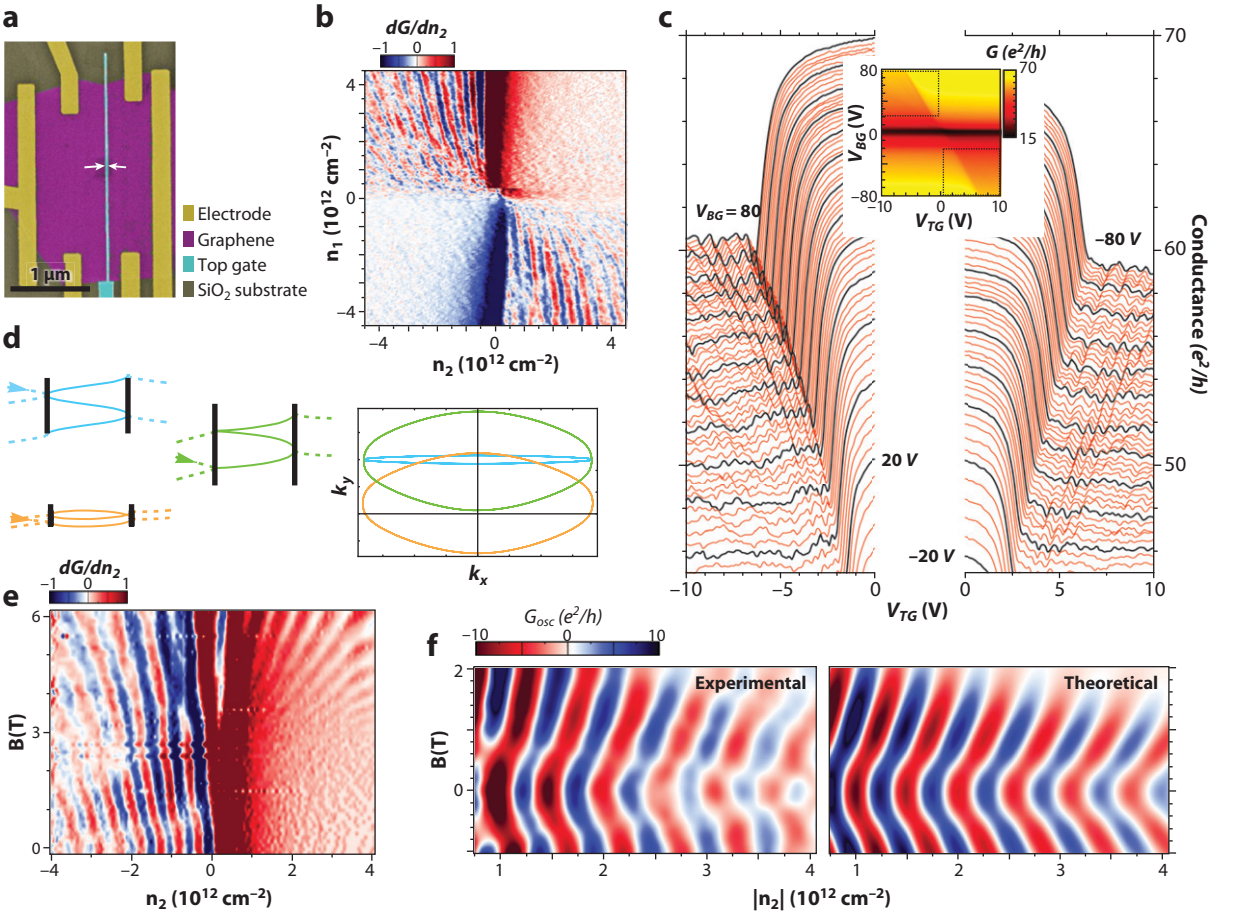

Figure 4

(*a*) Scanning-electron microscopy image of a typical graphene heterojunction device. Electrodes, graphene, and top gates are represented by yellow, purple, and cyan, respectively. The samples sit on a 285-nm SiO_2 substrate. The top gate in this device is ~20 nm wide (*white arrows*). (*b*) Differential transconductance map of the device as a function of densities n_1 and n_2 in the graphene lead and locally gated region, respectively. Interference fringes appear in the presence of p-n junctions, which define the Fabry-Perot cavity. (*c*) (*Inset*) Conductance map of the device in the V_{BG}-V_{TG} plane. The main panels show cuts through this color map in the regions indicated by the dotted lines in the inset, showing the conductance as a function of V_{TG} at fixed V_{BG}. Traces are separated by a step in V_{BG} of 1 V, starting from 80 V with traces taken at integer multiples of 5 V in black. (*d*) Schematic diagram of trajectories contributing to quantum oscillations in real and momentum space. The dominant modes at low magnetic field (*blue*) give way, with increasing B, to phase-shifted modes with negative reflection amplitude due to the inclusion of the nontrivial Berry phase (*orange*), near $k_y = 0$. The original finite k_y modes are not yet phase shifted at B_c (*green*), but owing to collimation, they no longer contribute to the oscillatory conductance. (*e*) Magnetic-field and density dependence of the transconductance. (*f*) Oscillating part of the conductance at $V_{BG} = 50$ V for low fields. G_{osc} as extracted from the experimental data over a wide range of densities and magnetic fields (*left*) matches the behavior predicted by a theory based on realistic simulation of the heterojunction electrostatics including nonlinear screening (5). The phase shift due to Klein tunneling (81) is responsible for the "kink" in the oscillations observed at a few hundred milliTesla (*right*). Reproduced from Reference 64.

$$G_{osc} = e^{-2L/l_{LGR}} \frac{4e^2}{h} \sum_{k_y} 2|T_+|^2|T_-|^2 \; R_+R_-\cos(\theta_{WKB}), \qquad 6.$$

where $T_\pm$ and $R_\pm$ are, respectively, the transmission and reflection amplitudes at $x = \pm L/2$, θ_{WKB} is the semiclassical phase difference accumulated between the junctions by interfering trajectories, and ℓ_{LGR} is a fitting parameter that controls the amplitude of the oscillations.

At zero magnetic field, particles are incident at the same angle on both junctions, and the Landauer sum (6) is dominated by the modes for which both transmission and reflection are nonnegligible, so neither normal nor highly oblique modes contribute. Instead, the sum is dominated by modes with finite k_y, peaked at approximately $k_y = \pm\sqrt{F\ln(3/2)}\pi\hbar v_F$. As the magnetic field increases, cyclotron bending favors the contribution of modes with $k_y = 0$, which are incident on the junctions at angles with the same magnitude but opposite sign (**Figure 4*c***). If perfect transmission at zero angle exists, then analyticity of the scattering amplitudes demands that the reflection amplitude change sign as the sign of the incident angle changes (81), causing a π shift in the reflection phase. This effect can also be described in terms of the Berry phase: The closed momentum space trajectories of the modes dominating the sum at low field and high k_y do not enclose the origin, whereas those at intermediate magnetic fields and $k_y \sim 0$ do. As a consequence, the quantization condition leading to transmission resonances is different owing to the inclusion of the Berry phase when the trajectories surround the topological singularity at the origin, leading to a phase shift in the observed conductance oscillations as the phase-shift-containing trajectories begin to dominate the Landauer sum (6).

Young & Kim (64) reported experimental realization of the coherent electron transport in pnp (as well as npn) graphene heterojunctions. The key experimental innovations were to use an extremely narrow ($\leq$ 20 nm wide) top gate, creating a Fabry-Perot cavity between p-n junctions smaller than the mean free path, which was $\sim$ 100 nm in the samples studied. **Figure 4*a*** shows the layout of a graphene heterojunction device controlled by both top-gate voltage (V_{TG}) and back-gate voltage (V_{BG}). The conductance map shows clear periodic features in the presence of p-n junctions, which appear as oscillatory features in conductance as a function of V_{TG} at fixed V_{BG} (**Figure 4*b***). For the electrostatics of the devices presented in this device, the magnetic field at which this phase shift is expected to occur is in the range $B^* = 2\hbar k_y/eL \sim$ 250–500 mT, in agreement with experimental data that show an abrupt phase shift in the oscillations at a few hundred milliTesla (**Figure 4*d***). Experiments can be matched quantitatively to the theory by calculation of Equation 6 for the appropriate potential profile, providing confirmation of the Klein tunneling phenomenon in graphene.[1] As the magnetic field increases further, the ballistic theory predicts the disappearance of the FP conductance oscillations as the cyclotron radius shrinks below the distance between p-n junctions, $R_c \lesssim L$, or $B \sim 2$ T for the devices considered in Reference 64.

There is an apparent continuation of the low-magnetic-field FP oscillations to Shubnikov-de Haas (SdH) at high magnetic fields. Generally, the FP oscillations tend to be suppressed at high magnetic fields as the cyclotron orbits get smaller than the junction size. By contrast, disorder-mediated SdH oscillations become stronger at high magnetic field owing to the large separation between Landau levels. The observed smooth continuation between these two oscillations does not occur by chance. FP oscillations at magnetic fields higher than the phase shift are dominated by trajectories with $k_y = 0$. Similarly, SdH oscillations, which can be envisioned as cyclotron orbits beginning and ending on the same impurity, must also be dominated by $k_y = 0$ trajectories (83). The result is a seamless crossover from FP to SdH oscillations. This is strongly dependent

[1]Strictly speaking, although the phase shift is a consequence of Klein tunneling, the observation of the phase shift does not imply identically zero reflection at $\theta = 0$, only that the real part of the reflection amplitude becomes very small.

on disorder concentration: For zero disorder, SdH oscillations do not occur, whereas for very strong disorder SdH oscillations happen only at high fields and FP oscillations do not occur as a result of scattering between the p-n junctions. For low values of disorder such that SdH oscillations appear at fields much smaller than the phase-shift magnetic field, B_c, the two types of coherent oscillations could, in principle, coexist with different phases. The role of disorder in the FP-SdH crossover has only begun to be addressed experimentally (64) and theoretically (39).

Several other groups (61, 62) conducted similar experiments on at least partially phase-coherent graphene heterojunctions, although they did not observe the phase shift that is the signature of Klein tunneling. Further theoretical considerations of quantum transport across pnp junctions in the presence of disorder were discussed by Rossi et al. (84), who calculated the resistance and the Fano factor in the presence of weak disorder, both of which show broad resonance peaks due to the presence of quasibound states. As expected from the phenomenological model described in Equation 6, these features are washed out when the mean free path becomes of the order of the distance between the two p-n interfaces.

Expanding the number of p-n-junction boundaries can be achieved simply by installing an array of top gates on graphene, producing a superlattice electrostatic potential. Although this has not been demonstrated experimentally owing to constraints on sample quality, multiple theoretical studies of graphene p-n junction arrays exist (65–68, 71, 85–89). In the simple case of 1D periodic Dirac delta function barriers of strength P whose potential is given by $V(x, y) = \hbar v_F P\delta(x)$, Barbier et al. (89) showed that the dispersion relation of this Kronig-Penney model of a superlattice is a periodic function of P and causes collimation of an incident electron beam for $P = 2\pi n$, where n is an integer. For a Kronig-Penney superlattice with an alternating sign of the height of the barriers, the Dirac point in the 2D dispersion becomes a Dirac line for $P = \pi(n+1/2)$. The modification of the graphene spectrum remains an interesting direction to pursue experimentally.

Superlattices can also have a supercollimating effect on ballistically propagating carriers, creating an electron beam with virtually no spatial spreading or diffraction. The unit transmission of normally incident carriers means that, in a sample with minimal scattering, a highly collimated electron beam can be created without a waveguide or external magnetic fields (65). Such a perfect collimation stems from the creation of a chiral quasi-1D metallic state originating in the collapse of the intrinsic helical nature of the charge carriers in the superlattice potential.

In realistic graphene devices, however, disorder dominates, and any experimental superlattice will need to be analyzed with this in mind. The conductance of disordered graphene superlattices with short-range structural correlations has been studied theoretically (86, 88). Ignoring intervalley scattering, these studies demonstrated that the transport and spectral properties of such structures are strongly anisotropic even in the presence of disorder. In the direction perpendicular to the barriers, the eigenstates in a disordered sample are delocalized for all energies and provide a robust minimum nonzero conductivity. Along with extended states, however, there exist discrete sets of angles and energies with exponentially localized eigenfunctions, producing disorder-induced resonances. It is particularly interesting that the disorder not only suppresses the transmission of carriers across the barriers but, counterintuitively, can also enhance transmission.

6. TRANSPORT AT HIGH MAGNETIC FIELDS: QUANTUM HALL EFFECT IN GRAPHENE HETEROJUNCTIONS

In the limit of the well-separated graphene p-n junctions, electron density is relatively uniform far away from the junctions. At sufficiently high magnetic fields, therefore, both graphene leads

and the locally gated region can develop independent QH effects if the density and magnetic field are tuned to filling factor ν corresponding to an integer number of filled (possibly degenerate) Landau levels. At the interfaces between these regions, however, the edge states come into contact with each other, leading to inter-edge state scattering and an anomalous two-terminal conductance, which appears to be quantized at rational fractional values of e^2/h. Owing to the mismatch between the numbers of edge states in the different filling fraction regions, the transport in such heterogeneous devices is governed by the mixing of the edge states at the boundary and can be calculated using a simple scattering matrix approach for the finite channels carrying current in and out of the boundary region (90). Electronic transport through regions with different filling factors was studied as GaAs heterostructures more than 20 years ago (91). Graphene is distinct because researchers can observe the QH effect in both electrons and holes. In addition, these regions are adjacent without a large depletion region separating them at a graphene p-n junction. Edge-state conduction in a pnp or npn device provides a richer physics than that of the unipolar two dimensional electron gas, leading to a new regime of total edge-state mixing and equilibration.

We first consider QH physics for a single p-n junction in the QH regime, a subject that has been studied both experimentally and theoretically (59, 90). In the unipolar regime, the edge states circulate in the same direction at the interface between regions of different filling and conductance is determined by the edge channels that exist in both regions: $g_{pp} = (2e^2/h)\min(|\nu_1|,|\nu_2|)$, where ν_1 and ν_2 are the filling fraction of each region. In the bipolar regime ($\nu_1\nu_2 < 0$), in contrast, the edge states propagate in opposite directions on opposite sides of the p-n boundary, bringing electrons and holes from different reservoirs to the p-n interface. This interface evinces complete mode mixing, so that the two-terminal conductance is $g_{pn} = (2e^2/h)|\nu_1||\nu_2|/(|\nu_1| + |\nu_2|)$. Note that in single-layer graphene, the filling fractions ν_1 and ν_2 take integer values ($\pm 2, \pm 6, \pm 10, \cdots$), leading to fractional values of the quantum of conductance for g_{pn} in the bipolar regime (see **Figure 5**). The resulting fractionally quantized plateaus have nothing to do with the interaction-driven fractional QH effect, but rather, they are the result of nontrivial addition of a discrete set of current carrying modes in each arm of the device.

Further unusual QH conductance plateaus appear in conductance measurements of pnp heterojunctions at high magnetic fields (60). Depending on the induced carrier densities, this device can operate as either a *pnp*, *npn*, *pp′p*, or *nn′n*, where $p(n)$ represents hole (electron) majority carriers and the prime symbol indicates the same polarity of carrier but different density in the locally gated region. As both the local-gate voltage (V_{LG}) and back-gate voltage (V_{BG}) tune the density of the local (back) gate region n_2 (n_1), a series of fractional QH conductance plateaus appears (see **Figure 5**). Similar to the QH transport in a single p-n junction, this double-junction QH transport can be understood by edge-state mixing at the boundary of the different regions. In this system, the transport can be categorized into three different regimes depending on the relative magnitude and sign of the carriers in each region of the lateral heterojunctions: (*a*) edge-state transmission regime ($|p|>|p'|$ or $|n|>|n'|$), (*b*) partial-equilibrium regime ($|p|>|p'|$ or $|n|<|n'|$), and (*c*) full-equilibration regime (*pnp* or *npn*). Similar to the analysis of a single p-n junction, the edge-state transmission and mixing results are $g_{(i)}=(2e^2/h)|\nu'|$ and $g_{(iii)} = (2e^2/h)|\nu||\nu'|/(2|\nu| + |\nu'|)$. Interestingly, in the partial-equilibration regime, where there are more edge states in the locally gated region than in the graphene leads, the situation is distinct from that occurring in the case of a single p-n junction. Here, the states circulating in the locally gated region can produce partial equilibration among the different channels, because they couple modes with different electrochemical potentials. A detailed analysis considering both current conservation and partially equilibrated edge-state circulation (60) yields $g_{(ii)} = (2e^2/h)|\nu||\nu'|/(2|\nu| - |\nu'|)$ for $|p'|>|p|$ or $|n'|>|n|$. We note that this partial-equilibration

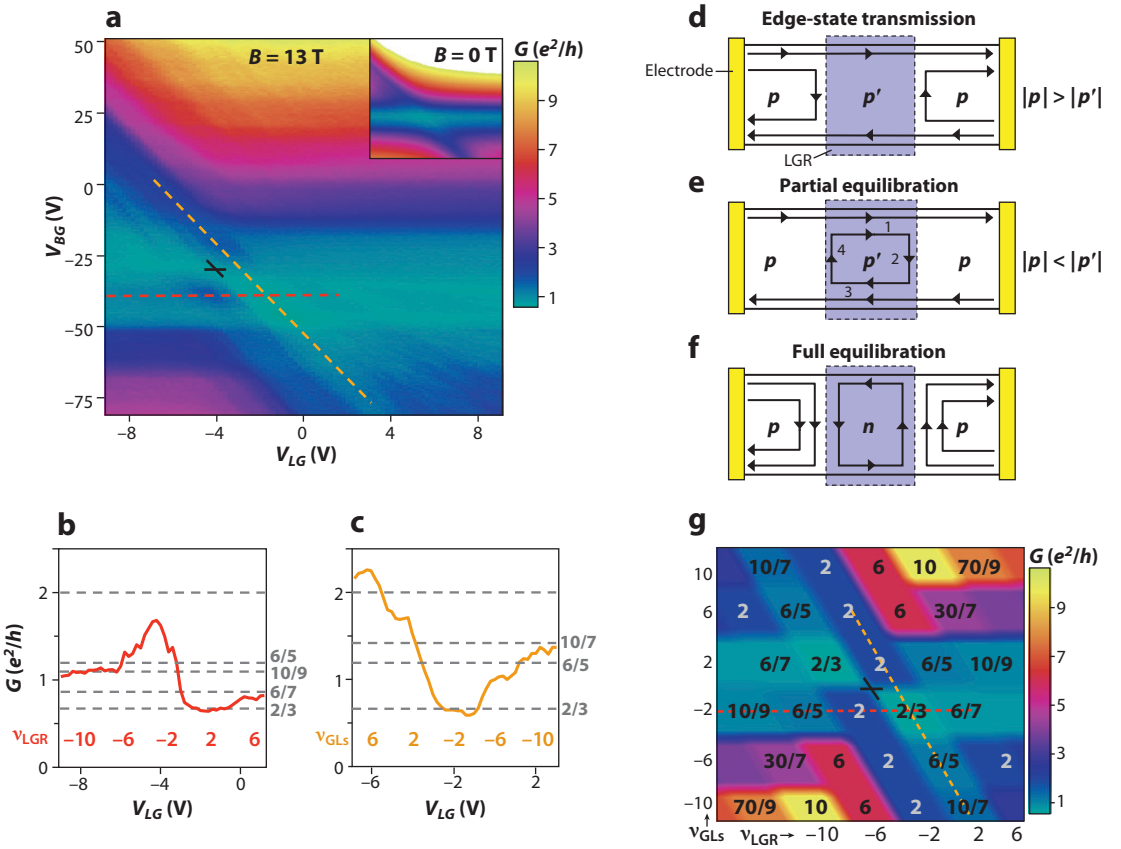

Figure 5

(*a*) Color map of conductance $G(V_{LG}, V_{BG})$ at magnetic field $B = 13$ T and $T = 4.2$ K. The black cross indicates the location of filling factor zero in the locally gated region (LGR) and graphene leads (GLs). Inset: Conductance at zero B in the same V_{LG}-V_{BG} range and the same color scale as main figure (*white* denotes $G > 10e^2/h$). (*b*) $G(V_{LG})$ trace along the dashed red line in panel *a* showing quantized fractional values of the conductance quantum. Numbers on the right indicate expected fractions for the various filling factors. (*c*) $G(V_{LG})$ trace along the dashed orange line in panel *a*. Numbers below the traces in panels *b* and *c* indicate filling-factor LGR and GLs, respectively. (*d*, *e*, *f*) Edge-state diagrams representing possible equilibration processes taking place as the density in the LGR and GLs are tuned between positive (*p* or *p*′) and negative (n). The center blue region indicates the LGR. Left and right yellow boxes indicate contact electrodes. (*g*) Simulated color map of the theoretical conductance plateaus expected from the mechanisms shown in panels *d*, *e*, and *f* for different filling factors in the GLs and LGR. The numbers in the rhombi indicate the conductance at that plateau. The color scale is identical to that of panel *a*. Reproduced from Reference 60.

regime can occur only in the presence of two *nn*′ or *pp*′ interfaces and would not occur in a single junction device (59). Similar results were obtained later in higher quality graphene heterojunction devices employing a contactless air bridge for the top gate (61, 92).

More recently, Ki et al. (93) have investigated the dependence of longitudinal and diagonal resistances of a graphene p-n interface using multiterminal measurement configurations. They observed that the resistance of a p-n device in a four-terminal scheme is asymmetric with respect to the $\nu = 0$ in the whole device. This resistance asymmetry is caused by the chiral direction–dependent change in the equilibration position.

The presence of backscattering between opposite edges in the samples underneath bulk of the locally gated regime or in the transitional regions at the p-n junctions short the QH edge

states and degrade sharp quantization. Long et al. (94) investigated the stability of the quantized plateaus in the p-n junction in the presence of disorder using a Landauer-Buttiker formalism combined with the nonequilibrium Green function method. They found that the lowest plateau can survive for a very broad range of disorder strength, but the existence of plateaus corresponding to higher fillings in the various regions depends on system parameters, in excellent agreement with experimental data.

Park and collaborators (87) have theoretically discussed QH edge-state transport in graphene *pnpnpn*... superlattices. As in the case of zero magnetic field, the 1D potential modifies the graphene band structure, creating multiple band crossings at zero energy and so additional 1D Dirac points. Interestingly, the number of 1D Dirac points for this type of graphene supper lattice increases by two (without considering the spin and valley degrees of freedom) whenever the potential amplitude exceeds a value of $U_0^N = 4\pi N\hbar v_F/L$, where N is a positive integer and L is the repeating length scale of the superlattice. New zero-energy branches of massless fermions are generated with nearly the same electron-hole crossing energy as that of the original Dirac point of graphene. Due to these new zero-energy branches, the Landau levels at charge-neutral filling become $4(2N+1)$-fold degenerate (with $N = 0,1,2,\ldots$, tunable by the potential strength and periodicity) with the corresponding Hall conductivity σ_{xy} showing a step at values $4(2N+1)e^2/h$. Awaiting experimental observation, these theoretical predictions are robust against variations in the details of the external potential and provide measurable signatures of the unusual electronic structure of graphene superlattices.

7. INTERMEDIATE MAGNETIC FIELDS: LANDAU-LEVEL COLLAPSE

In the intermediate magnetic fields where the cyclotron orbit becomes smaller than the carrier mean free path, Landau-level quantization is appreciable but the QH effect does not yet emerge. In the presence of an inhomogenous potential profile such as exists in the presence of a local top gate, this regime provides an interesting arena in which to investigate the interplay between perpendicular magnetic and in-plane electric fields in graphene. In particular, Lukose and collaborators (38) noticed that the emergent Lorentz symmetry of the single-particle graphene Hamiltonian (Equation 1) allows for a transformation of magnetic into electric fields. They identified two regimes for a 1D linear potential $U(x) = -eEx$, in analogy with relativistic electromagnetism. For $\beta \equiv \frac{cE}{v_f B} < 1$, the electric field can be eliminated by a "Lorentz boost" in which the speed of light parameter is equal to the Fermi velocity in graphene, v_f. The electronic spectrum in this regime is discrete and is described by Landau levels with a spectrum modified by the in-plane electric field, $\varepsilon \propto \sqrt{Bn}(1-\beta^2)^{3/4}$. As the magnetic field is lowered, or the electric field increases, the Landau levels collapse, leading to a continuous spectrum for $\beta \geq 1$. In this regime, the magnetic field can be eliminated (39, 95), leading to the prediction of an anomalous magnetoconductance of ballistic graphene p-n junctions, $G(B) = (1-\beta^2)^{3/4}$. Unfortunately, experimental evidence for this is complicated by the increased importance of impurity scattering at intermediate and high magnetic fields (58).

This collapse of the Landau levels has other experimental consequences. In transport, SdH-type resonances occur when closed orbits fulfill a Bohr-Sommerfeld quantization condition $\int_{x_1}^{x_2} p_x(x)dx = \pi(n+1/2-\gamma)$, where x_1 and x_2 are the two classical turning points, n is an integer, and the Berry phase contribution γ is 1/2 for the Dirac fermions in graphene. In the presence of an inhomogenous potential, we can introduce the position-dependent Fermi momentum, $k_F(x) = (\varepsilon - U(x))/\hbar v_F$. Thus, we obtain

$$\int_{x_1}^{x_2} \sqrt{(\hbar k_F(x))^2 - (p_y - eBx)^2}\,dx = \pi\hbar n. \quad 7.$$

For linear $U(x)$, this gives the Landau-level spectrum (2) for $B > B_c$. As B approaches B_c, one of the turning points moves to infinity, indicating a transformation of closed orbits into open trajectories (40). The experimental consequence is that, in the presence of a potential barrier, SdH resonance, rather than tracing lines toward zero field and zero density, should abruptly terminate a finite magnetic field.

To realize the collapse of Landau levels in an electron system, several conditions must be met. First, it must be possible to create a potential barrier that is steep on the scale of the cyclotron orbit radius. Second, the system must be ballistic on this length scale to suppress the broadening of Landau levels due to disorder. The experimental observation of the Landau-level collapse in the intermediate magnetic field regime was reported (64) and explained (40) recently in the same devices in which FP oscillations are observed. The effect occurs in the unipolar regime, where the narrow potential barrier is repulsive and competes with magnetic confinement. Landau-level collapse corresponds to a deconfinement transition as the field is lowered. The observed transport measurements exhibit SdH oscillations, which, in the unipolar regime, abruptly disappear when the strength of the magnetic field is reduced below a certain critical value. This behavior is explained by the semiclassical analysis of the transformation of closed cyclotron orbits into open, deconfined trajectories (**Figure 6**).

Another experimental consequence of Landau-level collapse in graphene is a modification of cyclotron resonance in the presence of an in-plane electric field. Kohn's theorem for cyclotron resonance (96) states that for particles with a parabolic spectrum, in-plane fields—including those due to Coulomb interactions between particles—do not affect the cyclotron

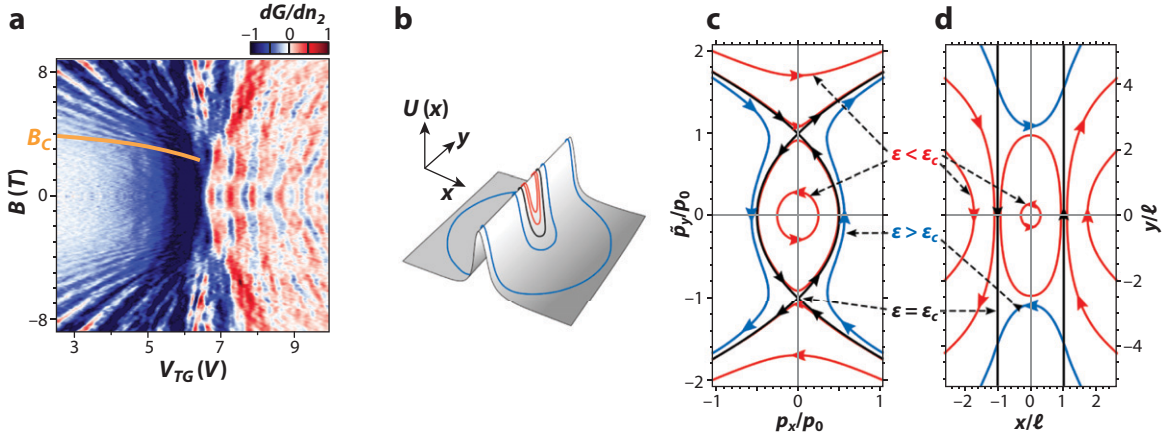

Figure 6

(*a*) dG/dV_{TG} as a function of B and V_{TG}. Shubnikov-de Haas (SdH) oscillations are observed at high B. The fan-like SdH pattern is altered by the barrier: In the $pp'p$ region it curves, weakens, and is washed out at fields $|B|<B_c$, whereas in the pnp region a crossover to Fabry-Perot oscillations occurs. Data are taken at $V_{bg} = 70$ V. (*b*) Closed orbits for the Thomas-Fermi potential obtained from the density profile, with $B = 9,7,5,3,1$ T and $p_y = 0$. Long trajectories, extending far outside the gated region, do not contribute to SdH oscillations as electrons scatter before completing an orbit. (*c*) Trajectories for the potential $U(x) = -ax^2$ and $p_y = 0$. Three types of trajectories are shown in momentum space (*b*) and position space (*c*): subcritical (*red*), critical (*black*), and supercritical (*blue*). The saddle points in momentum space correspond to motion along straight lines $x = \pm\ell_{MF}$, where the Lorentz force is balanced by the electric field. Reproduced from Reference 40.

resonance frequencies. This theorem rests on Galilean invariance of the single-particle continuum theory—a condition that is explicitly violated in graphene—and both theorists and experimentalists have taken this as cause to use cyclotron resonance as a probe of many body effects in graphene (97–99). The strong electric fields present in graphene p-n junctions, however, offer another venue in which to observe violation of Kohn's theorem.

The same Lorentz transformation used in Reference 38 to eliminate an in-plane electric field can be used to remove the built-in p-n electric field. In the presence of a time-dependent perturbation representing the electromagnetic radiation used to perform cyclotron resonance experiments, the result is a spatial dependence of the perturbation, $H' \propto e^{i\omega t} \rightarrow e^{i\omega(t-\beta x/v_F)}$. Expressing the coordinate in terms of creation and annihilation operators in the space of Landau levels, $\hat{a}$ and $\hat{a}^\dagger$, perturbation mixes all Landau levels, $H' \propto \sum_{n,m} c_{nm}(\hat{a})^n(\hat{a}^\dagger)^m$, with a suitable choice of the constants c_{nm} (100). The conclusion is that a static electric field changes the selection rules for cyclotron resonance, in addition to collapsing the spectrum. Although far-field cyclotron resonance measurements (99, 101) cannot hope to detect a signal from the tiny region of a p-n junction, there is some hope that newly available tip-assisted infrared spectroscopy (102) might be applied to probe this emergent quasirelativistic Lorentz physics in graphene.

8. CONCLUSIONS AND OUTLOOK

In this paper, we review the development and current status of electron transport in graphene heterojunction structures. In these devices, the unique linear energy dispersion relation and concomitant pseudospin symmetry are probed via the use of local electrostatic gates. Mimicking relativistic quantum particle dynamics, electron waves passing between two regions of graphene with different carrier densities will undergo strong refraction at the interface, producing an experimental realization of the century-old Klein tunneling problem of relativistic quantum mechanics. Many theoretical and experimental discussions were presented here, including peculiar graphene p-n and *pnp* junction conduction in the diffusive and ballistic regimes. Because electrons are charged, a magnetic field couples to them and its effects can be studied. We also discuss magnetotransport in graphene heterojunctions in various regimes, from the weak field limit, in which coherent FP oscillations are modified by semiclassical cyclotron bending, through the Landau-level collapse transition, and into the QH regime, in which edge-state mixing between electron and hole regions can be realized.

Device applications based on unusual electron transport in graphene heterojunctions have been discussed. In particular, in a ballistic graphene p-n junction, carrier trajectories experience strong refraction at the interface, which can be approximated by ray optics with a negative index of refraction. An interesting device configuration using this principle is the solid-state analog of the Veselago lens, where the region of negative index of refraction can focus and defocus electron waves propagating in the device (23). Still unexplored in the literature is the possibility that bilayer graphene may provide a better platform for this particular device concept. Whereas in single-layer graphene, absence of backscattering and exponential collimation place a high upper bound for the off current of the simplest Veselago lens device, electrons impinging on a bilayer graphene are perfectly reflected at normal incidence (2), leading to lower off currents. Moreover, progress toward band gap engineering in bilayer graphene makes it an even more promising venue to explore electronic optics.

In a coherent system, the electron waves can also interfere, producing quantum oscillations in the electrical conductance, which can be controlled through the application of both electric and magnetic fields. However, to integrate ballistic, phase-coherent quantum phenomena into a

useful device concept, one needs these properties to be robust over large length scales and at high temperatures. In typical graphene on SiO_2, however, mean free path and phase coherence length are usually limited to sub-100-nm length scales by long-range impurity scattering, and they are further decreased by substrate optical phonon scattering at high temperatures. In this regard, high-mobility, homogeneous graphene samples are extremely important for the realization of coherent graphene heterojunction devices. The recent development of high-mobility suspended samples (34, 35) as well as graphene on hexa-boron nitride (36, 79) has reignited hope in the possibility of room-temperature quantum coherence, as the intrinsic electron phonon coupling in graphene is weak and hBN has no low-lying optical phonon branches. The versatile platform of hBN dielectrics, in particular, allows for the long overdue realization of supercollimation in a graphene super lattice and ballistic bilayer heterojunctions.

Several other related charge transport phenomena in graphene heterostructures are not discussed in this review. These include the possibility of confinement via magnetic fields (103) and strain-induced pseudomagnetic fields (104) as well as snake states in inhomogenous magnetic fields (105, 106) and along graphene p-n junctions at finite magnetic fields, where elementary experimental demonstration has been shown (107). In addition, several theoretical proposals—such as valley filtering (108), guided plasmons (109), tunable Klein tunneling via spin-orbit interaction (110), and bilayer quantum coherent pnp junctions (111)—await even rudimentary experimental attacks. As device fabrication methods and sample quality improves, many of these proposals should become more feasible.

DISCLOSURE STATEMENT

The authors are not aware of any affiliations, memberships, funding, or financial holdings that might be perceived as affecting the objectivity of this review.

ACKNOWLEDGEMENTS

The authors thank B. Huard and D. Goldhaber-Gordon for helpful comments and for providing **Figure 3**.

LITERATURE CITED

1. Semenoff GW. 1984. *Phys. Rev. Lett.* 53:2449–52
2. Katsnelson MI, Novoselov KS, Geim AK. 2006. *Nat. Phys.* 2:620–25
3. Wallace PR. 1947. *Phys. Rev.* 71:622–34
4. Novoselov KS, Geim AK, Morozov SV, Jiang D, Katsnelson MI, et al. 2005. *Nature* 438:197–200
5. Zhang LM, Fogler MM. 2008. *Phys. Rev. Lett.* 100:116804
6. Ando T, Nakanishi T. 1998. *J. Phys. Soc. Jpn.* 67:1704–13
7. McEuen PL, Bockrath M, Cobden DH, Yoon Y-G, Louie SG. 1999. *Phys. Rev. Lett.* 83:5098–101
8. Novoselov KS, Geim AK, Morozov SV, Jiang D, Zhang Y, et al. 2004. *Science* 306:666–69
9. Zhang Y, Small JP, Pontius WV, Kim P. 2005. *Appl. Phys. Lett.* 86:073104
10. Bunch JS, Yuval Y, Brink M, Bolotin K, McEuen PL. 2005. *Nano Lett.* 5:287–90
11. Novoselov KS, Jiang D, Schedin F, Booth TJ, Khotkevich VV, et al. 2005. *Proc. Natl. Acad. Sci. USA* 102:10451–53
12. Berger C, Song Z, Li Ti, Li X, Ogbazghi AY, et al. 2004. *J. Phys. Chem.* 108:19912
13. Zhang Y, Tan Y-W, Stormer HL, Kim P. 2005. *Nature* 438:201–4
14. Geim AK, Novoselov KS. 2007. *Nat. Mater.* 6:183–91
15. Katsnelson MI. 2007. *Mater. Today* 10:20–27

16. Gusynin VP, Sharapov SG, Carbotte JP. 2007. *Int. J. Mod. Phys. B* 21:4611
17. Geim AK, MacDonald AH. 2007. *Phys. Today* 60:35
18. Katsnelson MI, Novoselov KS. 2007. *Solid State Commun.* 143:3–13
19. Geim AK, Kim P. 2008. *Sci. Am.* 298:90–97
20. Beenakker CWJ. 2008. *Rev. Mod. Phys.* 80:1337–54
21. Castro Neto AH, Guinea F, Peres NMR, Novoselov KS, Geim AK. 2009. *Rev. Mod. Phys.* 81:109–62
22. Das Sarma S, Adam S, Hwang EH, Rossi E. 2010. *Phys. Rev. B* 81:121408(R)
23. Cheianov VV, Fal'ko V, Altshuler BL. 2007. *Science* 315:1252–55
24. Hwang EH, Adam S, Das Sarma S. 2007. *Phys. Rev. Lett.* 98:186806
25. Martin J, Akerman N, Ulbricht G, Lohmann T, Smet JH, et al. 2008. *Nat. Phys.* 4:144–48
26. Zhang Y, Brar VW, Girit C, Zettle A, Crommie MF. 2009. *Nat. Phys.* 5:722–26
27. Chen J-H, Jang C, Adam S, Fuhrer MS, Williams ED, Ishigami M. 2008. *Nat. Phys.* 4:377–81
28. Adam S, Hwang EH, Galitski V, Sarma SD. 2007. *Proc. Natl. Acad. Sci. USA* 104:18392
29. Fradkin E. 1986. *Phys. Rev. B* 33:3257–62
30. Ludwig AWW, Fisher MPA, Shankar R, Grinstein G. 1994. *Phys. Rev. B* 50:7526
31. Ziegler K. 2007. *Phys. Rev. B* 75:233407
32. Tan Y-W, Zhang Y, Bolotin K, Zhao Y, Adam S, et al. 2007. *Phys. Rev. Lett.* 99:246803
33. Cheianov VV, Falko VI, Altshuler BL, Aleiner IL. 2007. *Phys. Rev. Lett.* 99:176801
34. Bolotin KI, Sikes KJ, Jiang Z, Klima M, Fudenberg G, et al. 2008. *Solid State Commun.* 146:351–55
35. Du X, Skachko I, Barker A, Andrei EY. 2008. *Nat. Nanotechnol.* 3:491–95
36. Dean CR, Young AF, Meric I, Lee C, Wang L, et al. 2010. *Nat. Nanotechnol.* 5:722–26
37. Cheianov VV, Fal'ko VI. 2006. *Phys. Rev. B* 74:041403
38. Lukose V, Shankar R, Baskaran G. 2007. *Phys. Rev. Lett.* 98:116802
39. Shytov A, Ruder M, Gu N, Katsnelson M, Levitov L. 2009. *Solid State Commun.* 149:1087–93
40. Gu N, Rudner M, Young A, Kim P, Levitov L. 2010. Landau level collapse in gated graphene structures. arXiv:1003.2399
41. Meric I, Han MY, Young AF, Ozyilmaz B, Kim P, Shepard KL. 2008. *Nat. Nanotechnol.* 3:654–59
42. Schwierz F. 2010. *Nat. Nanotechnol.* 5:487–96
43. Veselago VG. 1968. *Sov. Phys. Usp.* 10:509
44. Cserti J, Palyi A, Piterfalvi C. 2007. *Phys. Rev. Lett.* 99:246801
45. Piterfalvi C, Palyi A, Cserti J. 2009. *Phys. Rev. B* 80:075416
46. Dirac PAM. 1928. *Proc. R. Soc. Lond. Ser. A* 117:610–24
47. Klein O. 1929. *Z. Physik A Hadrons Nuclei* 53:157
48. Anderson CD. 1933. *Phys. Rev.* 43:491–94
49. Calogeracos A, Dombey N. 1999. *Contemp. Phys.* 40:313–21
50. Shytov AV, Katsnelson MI, Levitov LS. 2007. *Phys. Rev. Lett.* 99:246802
51. Silvestrov PG, Efetov KB. 2008. *Phys. Rev. B* 77:155436
52. Barraza-Lopez S. 2010. *Phys. Rev. Lett.* 104:076807
53. Huard B, Stander N, Sulpizio JA, Goldhaber-Gordon D. 2008. *Phys. Rev. B* 78:121402
54. Cayssol J. 2008. *Phys. Rev. Lett.* 100:147001
55. Cayssol J, Huard B, Goldhaber-Gordon D. 2009. *Phys. Rev. B* 79:075428
56. Mueller T, Xia F, Freitag M, Tsang J, Avouris P. 2009. *Phys. Rev. B* 79:245430
57. Lin Y-M, Dimitrakopoulos C, Jenkins KA, Famer DB, Chiu H-Y, et al. 2010. *Science* 327:662
58. Huard B, Sulpizio JA, Stander N, Todd K, Yang B, Goldhaber-Gordon D. 2007. *Phys. Rev. Lett.* 98:236803
59. Williams JR, DiCarlo L, Marcus CM. 2007. *Science* 317:638–41
60. Özyilmaz B, Jarillo-Herrero P, Efetov D, Abanin DA, Levitov LS, Kim P. 2007. *Phys. Rev. Lett.* 99:166804
61. Liu G, Jairo Velasco J, Bao W, Lau CN. 2008. *Appl. Phys. Lett.* 92:203103
62. Gorbachev RV, Mayorov AS, Savchenko AK, Horsell DW, Guinea F. 2008. *Nano Lett.* 8:1995–99
63. Stander N, Huard B, Goldhaber-Gordon D. 2009. *Phys. Rev. Lett.* 102:026807
64. Young AF, Kim P. 2009. *Nat. Phys.* 5:222–26

65. Park C-H, Son Y-W, Yang L, Cohen ML, Louie SG. 2008. *Nano Lett.* 8:2920–24
66. Pereira JM. 2006. *Phys. Rev. B* 74:045424
67. Bai C, Zhang X. 2007. *Phys. Rev. B* 76:075430
68. Pereira JM Jr, Vasilopoulos P, Peeters FM. 2007. *Appl. Phys. Lett.* 90:132122
69. Bai C, Yang Y, Zhang X. 2009. *Phys. Rev. B* 80:235423
70. Bai C, Yang Y, Zhang X. 2010. *Physica E* 42:1431–34
71. Pereira JM Jr, Peeters FM, Chaves A, Farias GA. 2010. *Semicond. Sci. Technol.* 25:033002
72. Sonin EB. 2009. *Phys. Rev. B* 79:195438
73. Fogler MM, Novikov DS, Glazman LI, Shklovskii BI. 2008. *Phys. Rev. B* 77:075420
74. Henriksen EA, Eisenstein JP. 2010. *Phys. Rev. B* 82:041412
75. Farmer DB, Chiu H-Y, Lin Y-M, Jenkins KA, Xia F, Abouris P. 2009. *Nano Lett.* 9:4474–78
76. Zou K, Hong X, Keefer D, Zhu J. 2010. *Phys. Rev. Lett.* 105:126601
77. Oostinga JB, Heersche HB, Liu X, Morpurgo AF, Vandersypen LMK. 2008. *Nat. Mater.* 7:151–57
78. Craciun MF, Russo S, Yamamoto M, Oostinga JB, Morpurgo AF, Tarucha S. 2009. *Nat. Nanotechnol.* 4:383–88
79. Young AF, Dean CR, Meric I, Sorgenfrei S, Ren H, et al. 2010. Electronic compressibility of gapped bilayer graphene. arXiv: 1004.5556
80. Özyilmaz B, Jarillo-Herrero P, Efetov D, Kim P. 2007. *Appl. Phys. Lett.* 91:192107
81. Shytov AV, Rudner MS, Levitov LS. 2008. *Phys. Rev. Lett.* 101:156804
82. Liang WJ, Bockrath M, Bozovic D, Hafner JH, Tinkham M, Park H. 2001. *Nature* 411:665–69
83. Vavilov MG, Aleiner IL. 2004. *Phys. Rev. B* 69:035303
84. Rossi E, Bardarson JH, Brouwer PW, Das Sarma S. 2010. *Phys. Rev. B* 81:121408
85. Park C-H, Yang L, Son Y-W, Cohen ML, Louie SG. 2008. *Nat. Phys.* 4:213–17
86. Bliokh YP, Freilikher V, Savelev S, Nori F. 2009. *Phys. Rev. B* 79:075123
87. Park C-H, Son Y-W, Yang L, Cohen ML, Louie SG. 2009. *Phys. Rev. Lett.* 103:046808
88. Abedpour N, Esmailpour A, Asgari R, Tabar MRR. 2009. *Phys. Rev. B* 79:165412
89. Barbier M, Peeters FM, Vasilopoulos P, Pereira JM. 2008. *Phys. Rev. B* 77:115446
90. Abanin DA, Levitov LS. 2007. *Science* 317:641–43
91. Haug RJ, MacDonald AH, Streda P, von Klitzing K. 1988. *Phys. Rev. Lett.* 61:2797
92. Velasco J Jr, Liu G, Bao W, Lau CN. 2009. *N. J. Phys.* 11:095008
93. Ki D-K, Nam S-G, Lee H-J, Vzyilmaz B. 2010. *Phys. Rev. B* 81:033301
94. Long W, Sun Q-f, Wang J. 2008. *Phys. Rev. Lett.* 101:166806
95. Shytov AV, Gu N, Levitov LS. 2008. *Solid State Comm.* 149:1087
96. Kohn W. 1961. *Phys. Rev.* 123:1242–44
97. Iyengar A, Wang J, Fertig HA, Brey L. 2007. *Phys. Rev. B* 75:125430
98. Bychkov YA, Martinez G. 2008. *Phys. Rev. B* 77:125417
99. Henriksen EA, Cadden-Zimansky P, Jiang Z, Li ZQ, Tung L-C, et al. 2010. *Phys. Rev. Lett.* 104:067404
100. Shizuya K. 2007. *Phys. Rev. B* 75:245417
101. Henriksen EA, Jiang Z, Tung L-C, Schwartz ME, Takita M, et al. 2008. *Phys. Rev. Lett.* 100:087403
102. Keilmann F, Hillenbrand R. 2004. *Philos. Trans. R. Soc. London Ser. A* 362:787–805
103. De Martino A, Dell'Anna L, Egger R. 2007. *Phys. Rev. Lett.* 98:066802
104. Pereira VM, Castro Neto AH. 2009. *Phys. Rev. Lett.* 103:046801
105. Oroszlány L, Rakyta P, Kormányos A, Lambert CJ, Cserti J. 2008. *Phys. Rev. B* 77:081403
106. Ghosh TK, De Martino A, Häusler W, Dell'Anna L, Egger R. 2008. *Phys. Rev. B* 77:081404
107. Williams JR. *Electronic transport in graphene: p-n junctions, shot noise, and nanoribbons*. PhD thesis. Harvard Univ., Cambridge, MA
108. Garcia-Pomar JL, Cortijo A, Nieto-Vesperinas M. 2008. *Phys. Rev. Lett.* 100:236801
109. Mishchenko EG, Shytov AV, Silvestrov PG. 2010. *Phys. Rev. Lett.* 104:156806
110. Yamakage A, Imura K-I, Cayssol J, Kuramoto Y. 2009. *EPL* 87:47005
111. Park S, Sim H-S. 2009. *Phys. Rev. Lett.* 103:196802

Annual Review of Condensed Matter Physics

Volume 2, 2011

Contents

Errata

An online log of corrections to *Annual Review of Condensed Matter Physics* articles may be found at http://conmatphys.annualreviews.org/errata.shtml